Ocean Modelling 102 (2016) 1–13

Contents lists available at ScienceDirect

Ocean Modelling

journal homepage: www.elsevier.com/locate/ocemod

Drag coefficient comparisons between observed and model simulated directional wave spectra under hurricane conditions

Yalin Fan*, W. Erick Rogers

Oceanography Division, Naval Research Laboratory, Stennis Space Center, MS 39529, United States

ARTICLE INFO

Article history:
Received 23 July 2015
Revised 3 February 2016
Accepted 16 April 2016
Available online 19 April 2016

Keywords:
Wind waves
WAVEWATCH III, Drag coefficient
Wave modeling
Tropical cyclones

ABSTRACT

In this study, Donelan, M.A., Babanin, A.V., Young, I.R., Banner, M.L., 2006. J. Phys. Oceanogr. 36, 1672–1688 source function is used to calculate drag coefficients from both the scanning radar altimeter (SRA) measured two dimensional wave spectra obtained during hurricane Ivan in 2004 and the WAVEWATCH III simulated wave spectra. The drag coefficients disagree between the SRA and model spectra mainly in the right/left rear quadrant of the hurricane where the observed spectra appear to be bimodal while the model spectra are single peaked with more energy in the swell frequencies and less energy in the wind sea frequencies. These results suggest that WAVEWATCH III is currently not capable of providing sensible stress calculations in the rear quadrants of the hurricane.

Published by Elsevier Ltd.

1. Introduction

Tropical cyclones, also popularly known as hurricanes or typhoons, are among the most spectacular and deadly geophysical phenomena. Both the most lethal and the most expensive natural disasters in U.S. history were tropical cyclones (Emanuel 2003). Tropical cyclones are driven by enthalpy fluxes from the sea and limited mostly by surface drag, but there is little understanding of the behavior of these fluxes at very high wind speeds. Direct measurements of the fluxes have been made at wind speeds as large as 25 m/s, but technical problems have thus far prevented reliable estimates at higher speeds. As a result, momentum transfer under extreme wind conditions has been extrapolated from these field measurements in a variety of modeling applications, including hurricane risk assessment and prediction of storm motion, intensity, waves and storm surges. However, work by Powell et al. (2003) and Donelan et al. (2004) suggests that in those extreme circumstances the drag decreases with wind speed or saturates. But, the understanding of the physics of such extreme events is only beginning.

Makin (2005) argues that spray production may give rise to the reduction of drag coefficient, C_d, by suppressing the air turbulence for increasing wind speed during hurricanes. On the other hand, Andreas (2004) has proposed that when spray returns to the water, short waves will be extinguished. This will no doubt reduce the drag considerably as the short waves carry most of the wave-induced stress (Makin and Kudryavtsev, 1999). Donelan et al. (2004) also suggest that flow separation may be the reason for drag reduction since the outer airflow does not "see" the troughs of the waves during such events and thus unable to follow the wave surface, and skips from breaking crest to breaking crest. All these hypotheses are standing on one common ground – the momentum flux is closely coupled with the sea state in the ocean.

Thus, fully coupled Atmosphere-wave-ocean model is suggested for accurate hurricane predictions as well as corresponding ocean responses (Chen et al., 2007; Fan et al., 2009a; Liu et al., 2011; Chen et al., 2013). Third generation wave models [e.g., WAVEWATCH III (Tolman, 1998), the Wave Model (WAM; Hasselmann et al., 1988), and Simulating Waves Nearshore (SWAN; Booij et al., 1999)] have been used to study surface wave responses during hurricanes, and the modeled wave parameters (significant wave height, mean/dominant wave length, mean/dominant wave direction) are shown to compare well with observations (Phadke et al., 2003; Moon et al., 2003; Xu et al., 2007; Fan et al., 2009b; Allard et al., 2014). Thus, there is desire in the modeling community to calculate momentum flux using the source function from the wave model. However, the wave energy spectrum computed by the models is from a balance between input and dissipation, and the wave parameters that are usually validated against observations are weighted by energy thus depend primarily on long waves around the peak. Since the momentum flux depends mainly on short wind waves, one may ask whether the model spectra represent real spectra well enough to provide reasonable momentum flux to atmosphere and ocean models in a coupled system for hurricane predictions, or is there a stronger argument for using parameterized fluxes?

* Corresponding author. Tel.: +0012286884655.
E-mail address: yalin.fan@nrlssc.navy.m, yalin.fan@gmail.com (Y. Fan).

http://dx.doi.org/10.1016/j.ocemod.2016.04.004
1463-5003/Published by Elsevier Ltd.

During Hurricane Ivan (SSHS category 4–5 in the Caribbean Sea and Gulf of Mexico) in 2004, detailed scanning radar altimeter (SRA) wave spectra measurements were collected by NASA through a joint effort between the NASA Goddard Space Flight Center and National Oceanic and Atmospheric Administration (NOAA)/ Atlantic Oceanographic and Meteorological Laboratory/Hurricane Research Division (HRD). The integrated parameters (significant wave height, dominant/mean wavelength and direction) calculated from the SRA spectra are used to evaluate WAVEWATCH III® by Fan et al. (2009) together with NDBC and satellite measurements, but the actual two-dimensional wave spectra produced by the wave models are not validated against observations.

In this study, these measured wave spectra will be used to calculate C_d using the source functions proposed by Donelan et al. (2006). The same source functions are applied to calculate C_d using model *simulated* wave spectra at the same time and location as the SRA spectra. Magnitude and spatial distribution of the C_d from both calculations are compared in detail. In particular, we investigate if the model spectra are suitable to provide reliable C_d for coupled models.

2. Methodology

2.1. The wave model

The wind-wave model, WAVEWATCH III® (WWIII) version 4.18, developed and used operationally at the National Centers for Environmental Prediction (NCEP) (Tolman et al., 2014) is used for this study. WWIII computes the evolution in space and time of the wave spectrum, which for the present study is discretized using 45 directions and 38 intrinsic (relative) frequencies extending from 0.02855 to 0.97 Hz, with a logarithmic increment of $f(n+1)=1.1f(n)$, where f(n) is the n^{th} frequency. The wave model is built on a latitude-longitude grid with a horizontal resolution of $1/12^{\circ}$.

Ocean currents obtained from the HYCOM + NCODA Global $1/12^{\circ}$ Reanalysis database (https://hycom.org/dataserver/glb-reanalysis) are introduced into WWIII. There are two significant ways the ocean current (U_c) impacts the wave field. First, through the wind input term in the calculation of the wind stress. When ocean current is present, the 10-m wind velocity input (U_{10}) is replaced by the relative wind velocity $U_{10}-U_c$. Second, the wave action equation, solved in WWIII accounts for the modulation by the ocean current such that the variable ocean current not only modifies the speed of the wave action flux but also any horizontal shear in the currents modifies the wave number of a particular wave packet as it propagates (Holthuijsen and Tolman, 1991, Fan et al., 2009b).

2.2. SRA measurements

Three sets of detailed SRA wave spectra measurements were collected by NASA. The flight tracks of the aircraft carrying the SRA are shown in Fig. 1. Two sets of measurements were collected from 1615 to 2010 UTC on September 9 and from 1040 to 1540 UTC on September 12 when Ivan was crossing the Caribbean Sea and at its maximum intensity of category 5. The third set of measurements was done from 2030 to 2353 UTC on September 14 when Ivan entered the Gulf of Mexico. The SRA measurements covered the region within about 2° of the hurricane eye. The SRA scanned a radar beam across the aircraft ground track to measure the elevation at 64 points on the sea surface. Sea surface topographic maps were produced from groups of SRA cross-track scan lines. The topography was then interpolated to a north- and east-oriented 256×256 rectangular grid of 7-m spacing centered on the data. The elevations in the uniform grid were transformed by a two-dimensional fast Fourier transform (FFT) with wavenumber spectral resolution of 0.0035 rad m^{-1}. The wave spectra were Doppler corrected and the 180° ambiguous spectral lobes were deleted (more details on the data process are given in Wright et al., 2001 and Walsh et al., 2002).

The horizontal resolution of the spectra is based on the altitude of the aircraft, and can resolve waves equal or longer than 50 m (~ 0.17 Hz) for the Hurricane Ivan measurements. Diagnostic tails need to be added in order to use these spectra for source function and momentum flux calculations. The method for adding the diagnostic tails and how this will affect the momentum flux calculations are discussed in Section 3.

2.3. Hurricane wind specification

The wind fields during Hurricane Ivan are obtained from the NOAA/HRD real-time wind analysis (HWIND) and interpolated into 0.5-h intervals using the normalized interpolation method given by Fan et al. (2009b). HWIND is an integrated tropical cyclone observing system in which wind measurements from a variety of observation platforms are used to develop an objective analysis of the distribution of 1-minute sustained wind speeds in a hurricane (Powell et al., 1998). It has the spatial resolution of about 6×6 km, covering an area of about $8^{\circ}\times8^{\circ}$ in latitude–longitude around the hurricane's center, and are provided at intervals of every 3 or 6 h. This frequency is not sufficient to force a numerical model and therefore the wind data are interpolated in space and time using the normalized interpolation method developed by Fan et al. (2009b).

2.4. Wind stress and drag coefficient calculation

The Janssen (1991) wind input parameterization is widely used in many studies and wave models including WWIII and the WAM model. In his theory, both the effects of waves and the effect of air turbulence on the mean wave profile are taken into account. An effective roughness z_e is proposed, which is used together with the friction velocity u_*, to determine the growth rate and hence the input source function. In numerical models, z_e and u_* from previous time step is used to determine the input source function, then the roughness length z_0, z_e, and u_* are solved using iterations of the wind speed log profile equation, expression of z_e, and the Charnock relationship (see details in Mastenbroek et al., 1993). This procedure is possible with the WWIII generated spectrum, but not practical for the SRA measurements. Thus a stress calculation based on the wave spectra and wind only is used for this study: Donelan et al. (2006). The authors proposed a wind input source function $S_{in}(f,\theta)$, based on field measurements collected during the Australian Shallow Water Experiment (AUSWEX):

$$S_{in}(f,\theta)=B(f,\theta)E(f,\theta) \tag{1}$$

where

$$B(f,\theta)=\gamma(f,\theta)\sigma\frac{\rho_a}{\rho_w} \tag{2}$$

and

$$\gamma(f,\theta)=G\sqrt{B_n'(f)}W(f,\theta) \tag{3}$$

The sheltering coefficient G is given by

$$G=2.8-\left\{1+tanh\left[10\sqrt{B_n'(f)}W(f,\theta)-11\right]\right\} \tag{4}$$

with

$$W(f,\theta)=\left\{max\left[0,\frac{U_{10}}{C}cos(\theta_{wv}-\theta_{wn})-1\right]\right\}^2 \tag{5}$$

Where, σ is the angular frequency, θ is the wave direction, $f=\sigma/2\pi$ is the frequency in hertz, ρ_a and ρ_w are air and water densities, θ_{wv} and θ_{wn} are wave and wind directions, and C is the

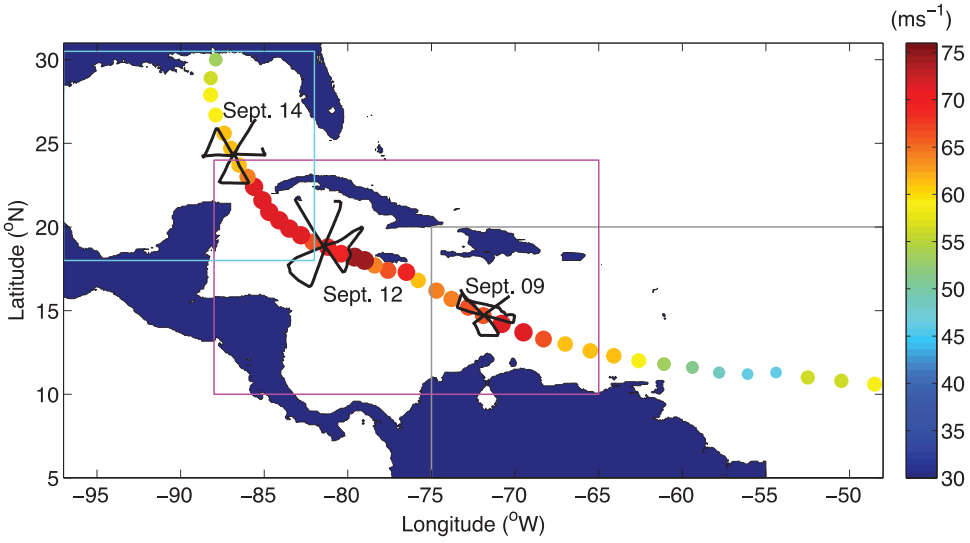

Fig. 1. Available scanning radar altimeter measurements along Hurricane Ivan track. The color and size of the circle represents the maximum wind speed of the hurricane. The black lines in the vicinity of the hurricane track represent the aircraft storm relative flight tracks during the SRA measurements. The gray, magenta, and cyan boxes indicate the model domain used for the September 9, 12 and 14 simulations. (For interpretation of the references to color in this figure legend, the reader is referred to the web version of this article.)

wave phase speed. The spectral saturation dimensionless variable is given as

$$B_n'(f) = A(f)B_n(f) = A(f)E(f)k^3C_g/2\pi \tag{6}$$

Here, k is the wave number, C_g is the group velocity, and $A(f)$ is a measure of narrowness of the directional distribution at a frequency

$$A^{-1}(f) = \int_0^{2\pi} E_n(f,\theta)d\theta \tag{7}$$

and the normalized directional spectrum equals

$$E_n(f,\theta) = \frac{E(f,\theta)}{E'(f)}, E'(f) = \max[E(f,\theta)] \tag{8}$$

The wave supported stress can then be calculated as

$$\tau_{wav} = \rho_w g \int_{f_0}^{f_e} \frac{S_{in}}{C} df \tag{9}$$

with f_0 and f_e (0.97 Hz is used in this study) being the beginning and ending frequency of the wave spectrum.

The total stress τ_{total} equals to τ_{wav} plus the viscous stress τ_v, which equals to

$$\tau_v = \rho_a C_v U^2 \tag{10}$$

where

$$C_v = max\left(-5\times10^{-5}U + 1.1\times10^{-3}, 0\right) \tag{11}$$

according to a fit to the Banner and Peirson (1998) laboratory observations by Tsagareli et al. (2010). The drag coefficient can then be estimated as

$$C_d = \tau_{total}/\rho_a U^2 \tag{12}$$

2.5. Swell energy calculation

The method of Hanson and Phillips (2001) is used for spectra partitioning in WWIII. A detailed partitioning implementation is described in Tracy et al. (2007). A wind sea fraction, W, is introduced for the partitioning,

$$W = E^{-1}E|_{U_p>c} \tag{13}$$

where E is the total spectral energy

$$E = \int_0^{2\pi}\int_0^{\infty} F(f,\theta)df d\theta \tag{14}$$

and U_p is the component of the wind in the wave direction multiplied by the wave age factor C_{mult}

$$U_p = C_{mult}U_{10}cos(\theta - \theta_u) \tag{15}$$

where U_{10} and θ_u are the magnitude and direction of the 10-m wind respectively. When U_p is larger than the local wave phase velocity c, locally generated waves dominate the wave spectrum. Thus, $E|_{Up>c}$ represents the energy in the wind sea part of the spectrum and $E - E|_{Up>c}$ gives the energy in the swell field. The wave age factor C_{mult} (Hanson and Phillips, 2001) is set at 1.7, which follows Tracy et al. (2007).

2.6. Parametric spectrum

Donelan et al. (1985) proposed a description of wind-generated deep water directional spectrum based on observations

$$F(\omega,\theta) = \frac{1}{2}\Phi(\omega)\beta sech^2\beta\left\{\theta - \bar{\theta}(\omega)\right\} \tag{16}$$

where $\bar{\theta}(\omega)$ is the mean wave direction and

$$\begin{aligned}&\beta = 2.61(\omega/\omega_p)^{+1.3};\ 0.56 < \omega/\omega_p\\ &\beta = 2.28(\omega/\omega_p)^{-1.3};\ 0.95 < \omega/\omega_p < 1.6\\ &\beta = 1.24;\ \text{otherwise}\end{aligned} \tag{17}$$

The frequency spectrum is

$$\Phi(\omega) = \alpha g^2\omega^{-5}(\omega/\omega_p)exp\left\{-\left(\frac{\omega_p}{\omega}\right)^4\right\}\gamma^{\Gamma} \tag{18}$$

with

$$\alpha = 0.006(U_c/c_p)^{0.55};\ 0.83 < U_c/c_p < 5 \tag{19}$$

$$\gamma = \begin{cases} 1.7;\ 0.83 < U_c/c_p < 1 \\ 1.7 + 6.0log_{10}(U_c/c_p);\ 1 \le U_c/c_p < 5 \end{cases} \tag{20}$$

$$\Gamma = exp\left\{-(\omega-\omega_p)^2/2\sigma^2\omega_p^2\right\} \tag{21}$$

Table 1
Model spectra data sets used in this study.

Data set	
A	Model spectra along SRA track at measurement time
B	Model spectra in 5 by 5 degree box centered at hurricane center
B-DT	High frequency part (> 0.17 Hz) of model spectra set B are replaced with diagnostic tails of $f^{-4.5}$
A-DT	High frequency part (> 0.17 Hz) of model spectra set A are replaced with diagnostic tails of $f^{-4.5}$
SRA	Scanning radar altimeter measured spectra
SRA-DT	High frequency diagnostic tails of f^{-4} are added to SRA spectra

Table 2
Model significant wave height (Hs) and dominant wave length (DLen) root mean square error (RMSE) and bias relative to SRA measurements.

	September 9		September 12		September 14	
	RMSE	Bias	RMSE	Bias	RMSE	Bias
Hs	1.08	0.42	1.38	0.88	1.22	0.37
DLen	37.54	−8.11	49.84	1.81	59.69	−26.46

and

$$\sigma = 0.08\left[1 + 4/(U_c/c_p)^3\right]; 0.83 < U_c/c_p < 5 \quad (22)$$

where, U_c is the component of the average 10 m wind in the mean direction of waves at the peak of $\Phi(\omega)$ and c_p is the phase speed at the spectral peak.

3. Diagnostic tails

Due to the spatial resolution, the SRA spectra can only resolve waves equal or longer than 50 m (~ 0.17 Hz). Diagnostic tails are added to the SRA spectra in order to use them for source function and momentum flux calculations in Section 4. Before doing this, it is necessary to investigate whether this use of a diagnostic tail will produce valid estimates of momentum flux. This is done through sensitivity analysis, applying the same approach to model spectra. Unlike SRA spectra, with the model spectra the higher frequencies (0.17–1 Hz) are known (since they are computed by the model) and so flux computations with the computed model high frequencies can be compared against flux computations where the model high frequencies have been replaced with a diagnostic tail.

Since exponential decay is used to specify winds outside the HRD wind field domain (Fan et al., 2009b), we limit our model domains to the extent of the HRD wind field as much as possible. WWIII is run independently for the September 9, 12 and 14 flight using model domains shown in Fig. 1. The model is run for three days before the flight time for all three simulations corresponding to the three sets of SRA measurements to allow the waves to fully develop in the model before they are compared with SRA measurements. Two sets of wave spectra are saved from all three simulations (Table 1). In set A, the model spectra are saved along the flight track at the SRA measurement time. In set B, the model spectra are saved at a snap shot in a 5 by 5 degree box centered at the hurricane center for spatial comparisons between models generated spectra and constructed spectra using diagnostic high frequency tails.

The significant wave height (Hs), dominant wave length (DLen), and dominant wave propagation direction (DDir) are calculated from model wave spectra set A. They compare very well with the SRA measurements (Fig. 2) as found by Moon et al. (2003) and Fan et al. (2009b). From the comparisons in Fig. 2 and the root mean square error and bias of the modeled Hs and DLen in Table 2, one might draw the conclusion that the wave model is doing a very good job predicting the wave field for hurricane Ivan. As we will show later that the model simulated wave spectrum can be very different from the observations, yet still give good comparison in these parameters.

Now, we will use model spectrum set B to demonstrate the difference between diagnostic tails and model calculated high frequency tail in terms of the drag coefficient, C_d. First, C_d is calculated using model spectra set B for all three simulations respectively using the Donelan et al. (2006) source function given in Section 2d (Fig. 3a, c, e). Then, the high frequency part (> 0.17 Hz) of the model spectra in set B is replaced with diagnostic tails of $f^{-4.5}$ to construct model spectra set B-DT (here DT stands for diagnostic tail) (Table 1). Both the magnitude and spatial distributions of the C_d calculated from model spectra set B-DT (Fig. 3b, d, f) are very similar to that calculated using model spectra set B. The spatial pattern correlations between the two C_d are 0.98, 0.99, and 0.94 for the September 9, 12 and 14 cases respectively. This suggests that adding diagnostic tails of $f^{-4.5}$ to the SRA spectra is a practical approach to construct complete wave spectra for stress calculations. Hence, we add diagnostic tails of $f^{-4.5}$ to the SRA spectra to construct SRA-DT spectra (Table 1) for analysis in Section 4. The diagnostic tail extends to the same upper frequency of the simulated spectrum (0.97 Hz).

4. Drag coefficient comparison

The high frequency part (> 0.17 Hz) of the model spectra set A are replaced with diagnostic tails of $f^{-4.5}$ to construct model spectra set A-DT (Table 1). C_d is calculated using model spectra set A and A-DT, and the constructed SRA spectra SRA-DT along all three flight tracks (Fig. 4). Notice that the C_d calculated from the reconstructed model spectra set A-DT match with that calculated from model spectra set A very well, indicating again that the diagnostic tail of $f^{-4.5}$ gives good estimate of the spectra in the high frequency range.

The model spectra set A-DT and the SRA-DT spectra will be used for the analysis from here on.

4.1. Model and SRA drag comparison

The C_d calculated from SRA-DT spectra follows that calculated from the model spectra A-DT with lower magnitude in general. However, the A-DT calculated C_d rapidly decreases when the flight heading is away from the center and reaches its minimum along the flight fragments highlighted by gray on Fig. 3, while the SRA-DT calculated C_d increases along these flight fragments (Gray highlighted area in Fig. 4). We can see that four of the flight fragments showing disagreements in C_d behavior are behind the hurricane, while one is in front of the hurricane during the September 9th flight and one is to the left of the hurricane during the September 12 flight. However, along these six flight fragments, the difference in modeled and measured Hs, DLen and DDir are not particularly large compare to the rest of the flight segments. Especially along the first and third flight fragments during the September 9th flight (Fig. 2), we see almost perfect match between model results and observations.

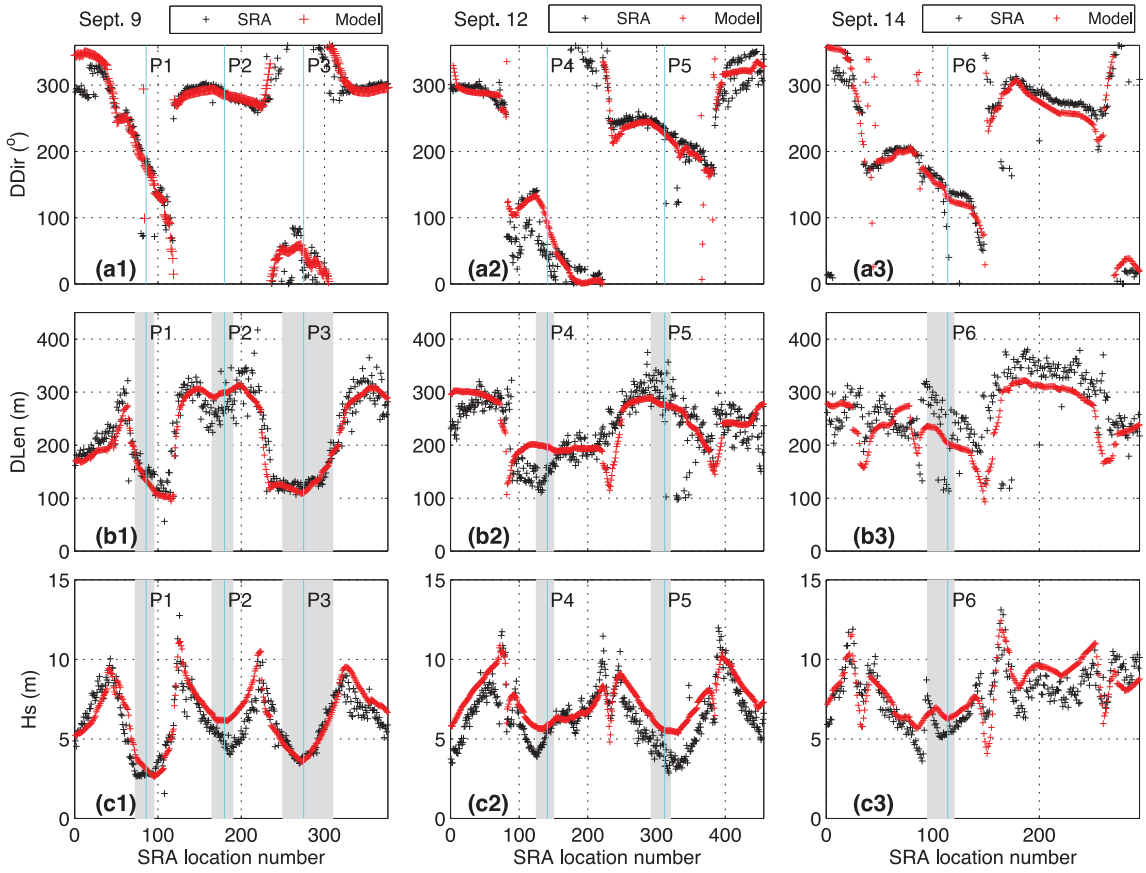

Fig. 2. Model results (red cross) compared with SRA measurement (black cross) along flight track for Dominant wave propagation direction (DDir), Dominant wave length (DLen), and Significant wave height (Hs) on September 9: (a1), (b1) and (c1); September 12: (a2), (b2) and (c2); and September 14: (a3), (b3), (c3). The gray areas are corresponding to the gray lines along the flight tracks on Fig. 3. The cyan lines indicate the location of the points defined along the flight tracks on Fig. 3. (For interpretation of the references to color in this figure legend, the reader is referred to the web version of this article.)

To further diagnose this, we picked one point on each of the six flight segments (white dots P1 to P6 shown in Fig. 3) to compare the directional wave spectrum between the model and the SRA measurement. At P1 to P5, the SRA spectrum calculated C_d are much larger than the model spectra calculated C_d (indicated by cyan line and magenta dot in Fig. 4), while the opposite is observed at P6. The model Hs, DLen and DDir are in good agreements with the SRA measurements at these six locations. Especially at point P1 and P3, where the model and SRA comparison are almost perfect (indicated by cyan line in Fig. 2a1–c1).

4.2. Model and SRA directional spectra comparison

Figs. 5 and 6 show the SRA directional wave spectra and the model spectra at points P1 to P6 along the SRA flight tracks (Fig. 3). Only the frequencies range within the SRA resolution (<0.17 Hz) are used for the model spectra plot. For the SRA spectra, the colors show 5% to 95% of the peak spectral density (SRA_{pk}) with 5% interval ($[0.05\times SRA_{pk} : 0.05\times SRA_{pk} : 0.95\times SRA_{pk}]$), and the black contour lines show every 10% increase from 10% to 90% ($[0.1\times SRA_{pk} : 0.1\times SRA_{pk} : 0.9\times SRA_{pk}]$). In order to make fair comparisons between the model and SRA spectra, we plot the model spectra differently: First, $[0.05\times SRA_{pk} : 0.05\times SRA_{pk} : 0.95\times SRA_{pk}]$ and $[0.1\times SRA_{pk} : 0.1\times SRA_{pk} : 0.9\times SRA_{pk}]$ are used to create the color contour maps and black contour lines for the model spectra at the same location. Then, the model spectra energy exceeds SRA_{pk} are plotted as color contour maps starting from SRA_{pk} at 5% increase interval until reach the peak model spectra density. The line of U_p / c equals to 1 are given on both spectra plots to help identify the swell and wind sea portion of the spectrum. Where c is the phase speed and U_p is the component of the wind in the wave direction multiplied by the wave age factor 1.7 (Eq. 15).

The model spectra have similar shapes at all six locations. Their peak energy densities are in the swell band and to the right of the wind direction at roughly 90° angle. The model wind sea energies do not have distinct peaks, and concentrated in a narrower frequency band (relative to the SRA spectra) that swirls out anticlockwise in directions.

The peak swell energies in the SRA spectra are much weaker than that in the model, but appear at similar frequency and direction, so the comparisons of DLEN and DDIR between model and SRA measurements give good agreements. However, the wind sea structures in SRA spectra are different at each location. Clearly defined distinct wind sea peak at similar frequencies as the swell peak are observed at point P1, P3, and P4, with wind sea energy lower than swell at P1, similar to swell at P3, and higher than swell at P4. Thus, when integrated over directions, the wind-sea spectral peak can be masked with the swell system energy. The wind sea spectrum at P1 also shows distinct peaks at higher frequencies than the swell peak, as well as P6. While the spectra at P2 only have a single peak in the swell band.

Wind sea directional spreading in the model spectra are similar to SRA measurements at point P1, P3, P4, and P6, and considerable larger at point P2 and P5, while wind sea energy in the model are generally lower than observations in low frequency band except at P4 and P6.

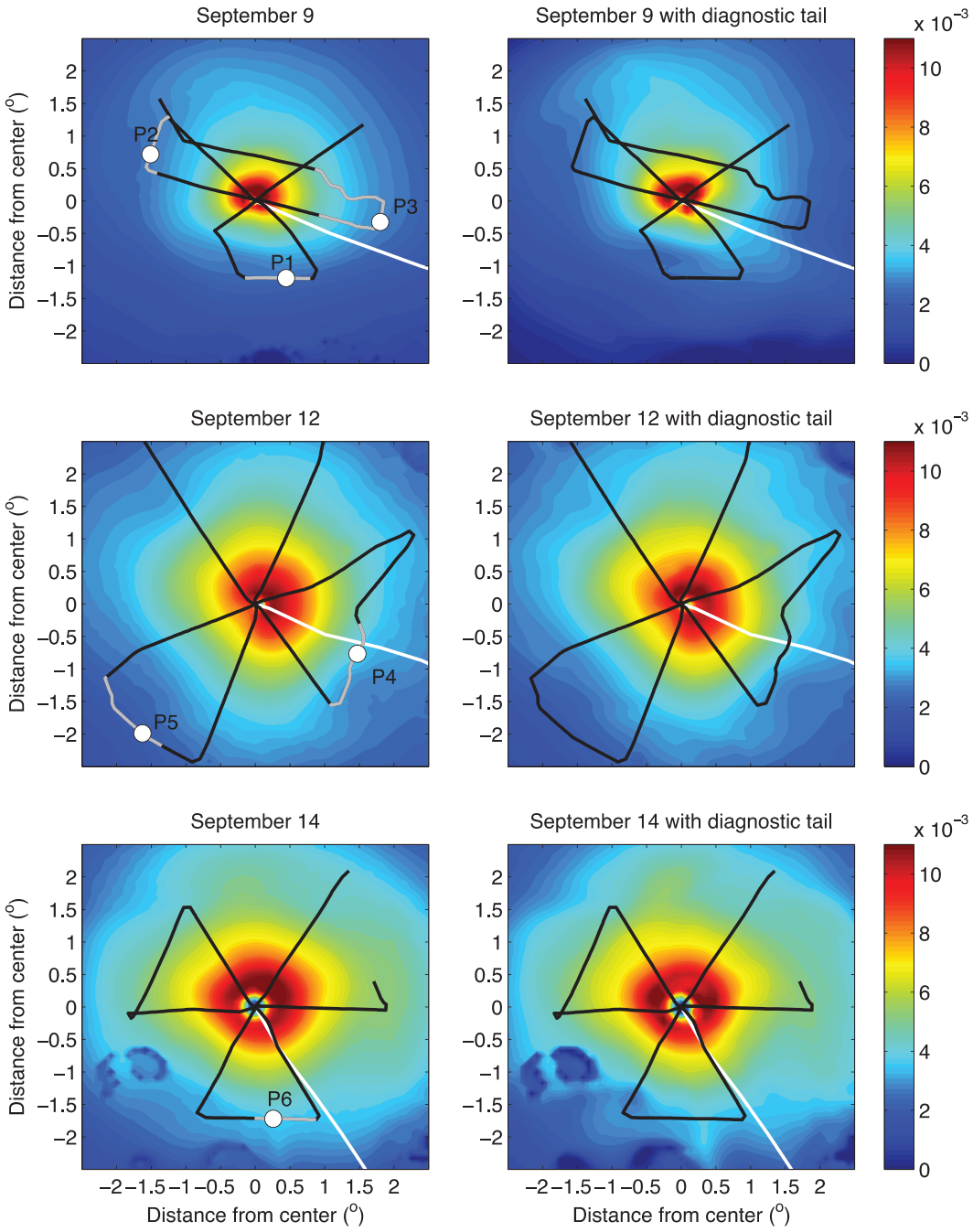

Fig. 3. Drag coefficient calculated using WWIII model spectra set B for (a) September 9, (c) September 12, and (e) September 14; and using constructed model spectra set C for (b) September 9, (d) September 12, and (f) September 14. The thick white line is the hurricane track, and the thick black line is the flight track for the SRA measurements. (For interpretation of the references to color in this figure legend, the reader is referred to the web version of this article.)

4.3. The effect of spectrum shape in drag calculations

Since the momentum flux is a vector sum of momentum contribution from all frequencies and directions, the very different behavior in the wind sea part of the model spectrum will result in a very different flux than that from the observed spectrum. The effect of spectrum shape in momentum flux calculations are demonstrated in Fig. 7 using the Donelan et al. (1985) parametric spectrum (Section 2.6), which gives good approximation of one dimensional spectra under hurricane conditions (Young, 2006). 20 m/s wind is used to calculate the drag coefficient for all spectra. The original spectrum (Fig. 7a) is constructed under 20 m/s wind forcing with 20° wind-wave angle and 90° directional spreading. The 10-m wind is applied at 20° angle to the left of the mean wave direction, which is typically observed in the SRA measurements (Figs. 5 and 6). The drag coefficient for this spectrum is 1.86×10^{-3}, and consistent with the C_d values in Fig. 4. For the same $\Phi(\omega)$, increase in directional spreading significantly decreases C_d to 1.12×10^{-3} (Fig. 7c); while keep the same spectrum but increase the wind-wave angle by 25° decreases C_d by ~30% (Fig. 7b). Keep the same directional spreading, and increase the wind sea peak energy density by 60% result in a drag increase of more than 100% (Fig. 7d). So, for single peaked spectrum, larger directional spreading and wind-wave angle will reduce C_d while increase in wind sea energy will increase the drag.

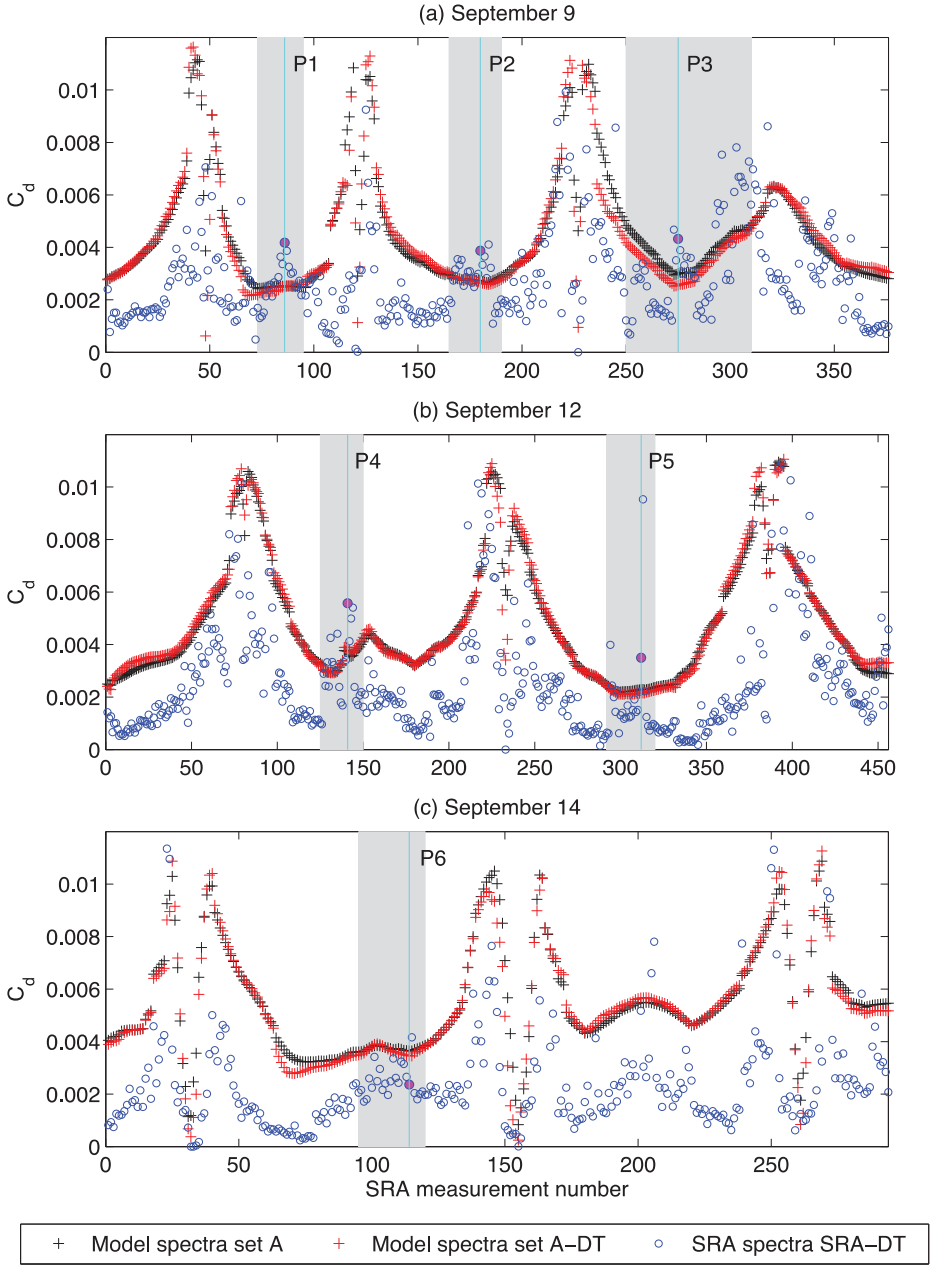

Fig. 4. Drag coefficient (C_d) calculated from model spectra set A (black cross), constructed model spectra set A-DT (red cross), and constructed SRA spectra SRA-DT (blue circle) using the Donelan et al. (2006) source function along the flight track of (a) September 9, (b) September 12, and (c) September 14. The gray areas are corresponding to the gray lines along the flight tracks on Fig. 3. The cyan lines indicate the location of the points defined along the flight tracks on Fig. 3. The SRA-DT spectra calculated C_d values at these points are highlighted by magneta. (For interpretation of the references to color in this figure legend, the reader is referred to the web version of this article.)

The effect of multiple peaks is also studied. First, the spectrum in Fig. 7a is rotated anticlockwise by 45° and added to the original spectrum to create a two-peak spectrum at the same frequency (Fig. 7e). The C_d for this spectrum is 2.49×10^{-3}. Then the spectrum in Fig. 7c is added to itself to create a single peak spectrum that has the same energy and directional spreading as the two-peak spectrum (Fig. 7f), but produces a lower C_d of 2.23×10^{-3} for the same wind vector. Note that this outcome also depends on the wind direction relative to the center of the one peak/two peaks of the spectrum, which is not further investigated here.

Sensitivity experiment (not shown) with the parametric spectra proposed by Young (2006) based on hurricane measurements also show similar effects of spectra shape on drag calculation: increase of wind-wave angle will reduce the drag while increase of wind sea peak energy density will significantly increase the drag. Due to the limitation of this parameterization in directional spreading variations, the sensitivity of drag on spreading and multiple peaks are not investigated.

All discrepancies in C_d between the model results and SRA measurements can be explained by the finding in Fig. 7. At P1, the model and SRA spectra have similar directional spreading, but the wind sea energy is higher in the SRA spectrum and thus results in a higher drag coefficient. At P2, the model spectrum has a much larger spreading, which causes the decrease in C_d. At P3 and P4, both the spreading and energy level are similar between the model and SRA spectra, but the SRA spectra have two peaks and its wind-sea angle is also smaller than the model. Both effects contribute to

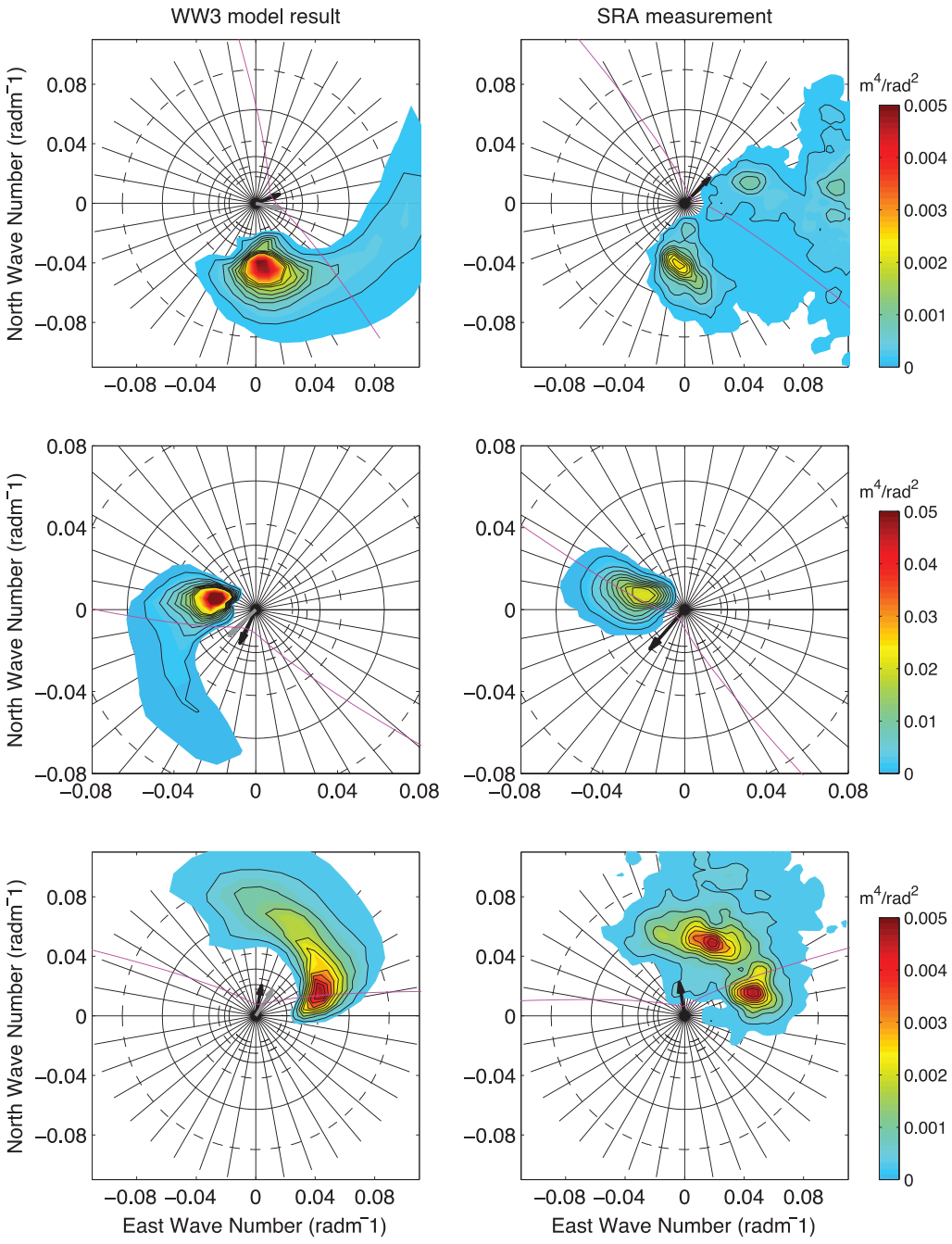

Fig. 5. Model (left) and SRA (right) directional wave spectra at point P1 (top), P2 (middle) and P3 (bottom) along the September 9th flight track defined in Fig. 3. For the SRA spectra, colors contours give 5% to 95% of the peak spectral density with 5% interval, and the black contour lines show every 10% increase from 10% to 90%. For the Model spectra, color contours are given using the same values for the SRA contours plus every 5% increment over the maximum SRA spectra value until the maximum Model spectra value, while the black contours lines are draw only for the SRA contour line values. The purple line shows U_p / c equals to 1. Only the frequencies range within the SRA resolution (<0.17 Hz) are used for the model spectra plot. (For interpretation of the references to color in this figure legend, the reader is referred to the web version of this article.)

create a larger C_d for the SRA spectra. At P6, the model spectrum has higher energy and smaller spreading than SRA spectrum. Both effects cause increase in drag, and thus the model drag is higher than SRA at this location. At P5, the model spectrum has bigger spreading and higher energy than the SRA spectrum. It seems like the decrease in drag due to larger spreading dominates over the increase in drag due to higher energy, and the ending results is a reduction in drag for the model spectrum.

Even though the characteristic of the wave spectrum at these six points are quite different, the comparisons at all these points suggest that the model spectrum tends to have higher energy in the swell frequencies and lower energy in the wind sea frequencies compared with observations. Even though the total wave energy corresponding to the spectra is close to that of the observations, the characteristics in the model resolved spectra are still far away from what is seen in the observations.

One possible reason for this discrepancy could be that the real hurricane wind field has fine structures that are not adequately represented by the HRD wind, which is an interpolated smooth wind field from limited observations.

It is also possible that the source function we used for the C_d calculations are developed under low to moderate wind conditions,

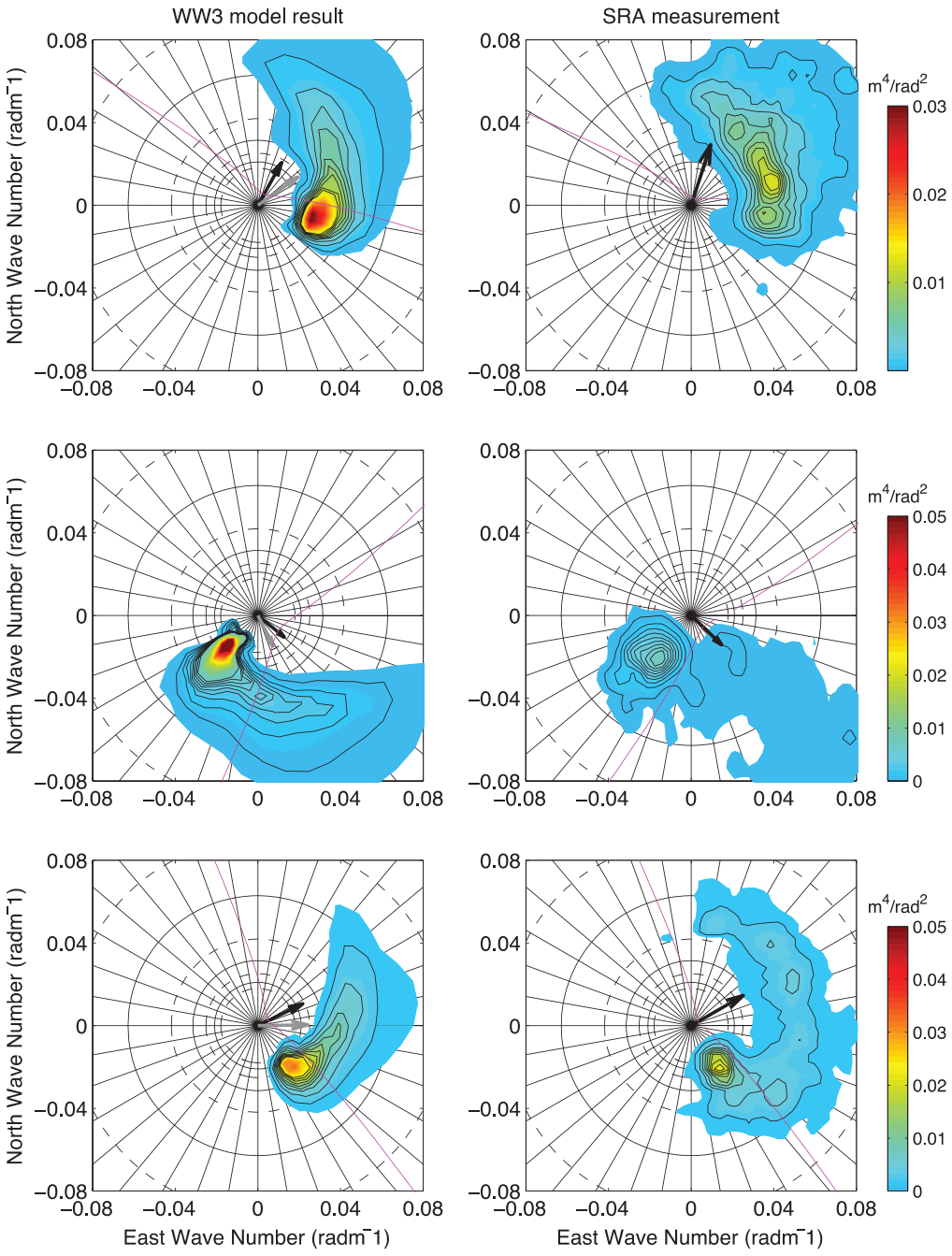

Fig. 6. Same as Fig. 5 but for point P4 and P5 along the September 12 flight track and point P6 on the September 14 flight track defined in Fig. 3.

and not suitable for high wind conditions such as the hurricanes. Donelan et al. (2012) proposed a new source function for wave modeling under hurricane conditions, and the calibration factors are determined from a comparison of modeled and observed significant wave height and mean period. The drag coefficients calculated using this source function (Appendix A) are much lower than that calculated using the Donelan et al. (2006) source function (for both model and SRA spectra), but the differences between the model and SRA spectra calculated drag coefficients show the same characteristics as we observed in Fig. 4.

Furthermore, the model may have too little dissipation for the swells and too much dissipation for the wind sea, such that it was able to resolve the peak frequency and direction of the swells reasonably well, while the wind sea part of the model spectra are continuous (unimodal) and narrower in frequency space compared to observations. This indicates a general behavior that is not expected: the model wind sea part is more problematic than the swells.

In developing wind seas, which is the case in hurricanes, most of the stress is determined by momentum transfer from wind to waves (Janssen, 1991). Having the correct wind sea spectra is essential for accurate stress calculations. Our wave modeling system (WW3 with HWIND) currently is not capable of providing realistic spectra and thus source function for stress calculations in the right/left rear quadrants of the hurricane.

5. Discussion

It is now widely accepted that the air-sea drag under a hurricane is closely coupled to the sea state in the ocean. Since the third

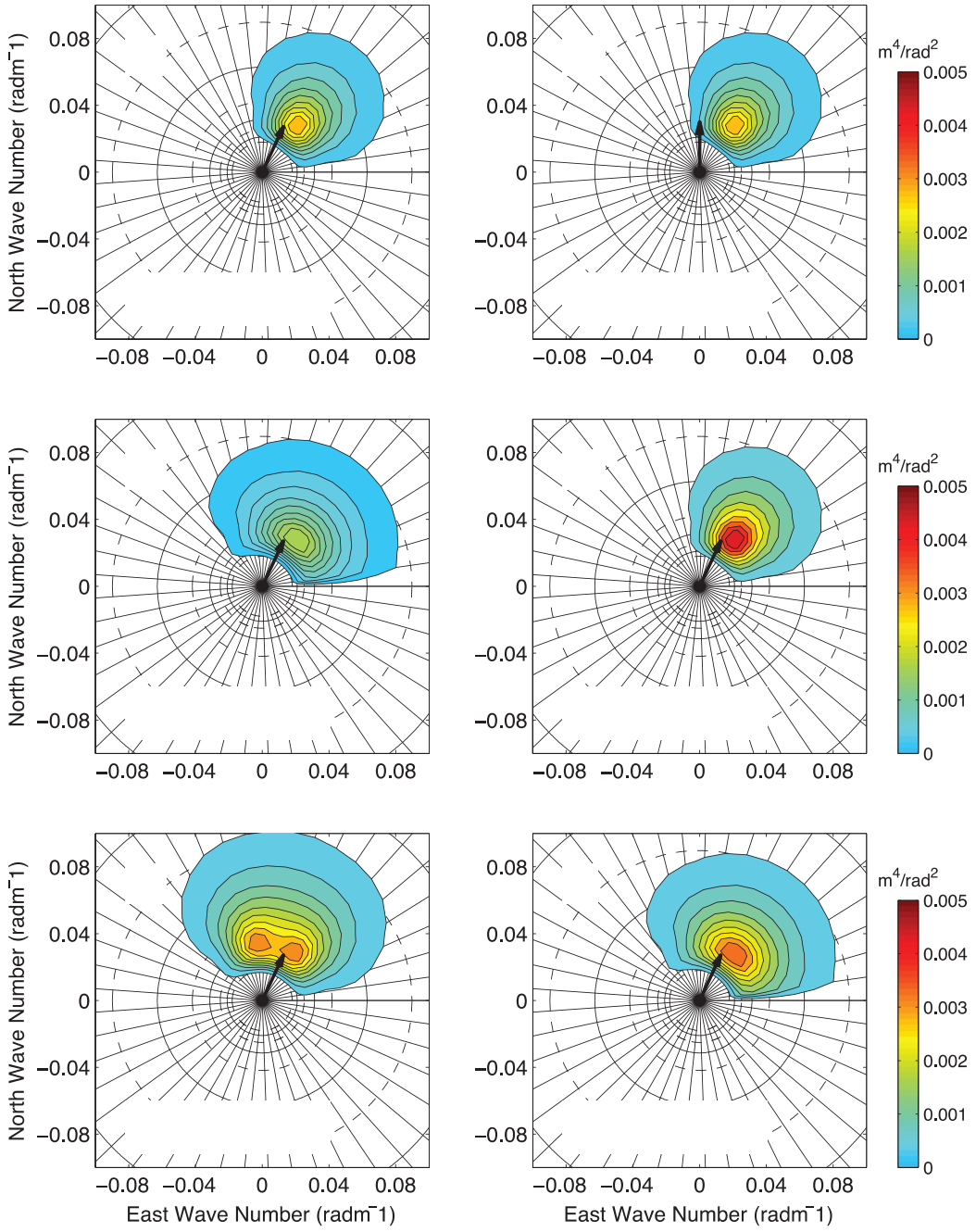

Fig. 7. Directional spectra generated using Donelan et al. (1985) under 20 m/s winds with 20° wind-wave angle and 90° directional spreading, (a) and (b); 20 m/s winds with 20° wind-wave angle and 135° directional spreading, (c); The spectrum in (c) is constructed by increasing the wind sea peak energy by 60% in (a). The spectrum in panel (e) is created by rotating the spectrum in (a) anticlockwise by 45° and add it to the spectrum in (a). The spectrum in panel (f) is created by adding the spectrum in (c) to itself. Colors and black contours give 10% to 90% of the peak spectral density with 10% interval. The numbers on the plots are drag coefficients for 20 m/s wind above the spectrum. The black arrow gives the wind direction. (For interpretation of the references to color in this figure legend, the reader is referred to the web version of this article.)

generation wave models (WAVEWATCH III, SWAN, and WAM) have been demonstrated to perform well in terms of bulk wave parameters under hurricane conditions by several studies (Phadke et al., 2003; Moon et al., 2003; Xu et al., 2007; Fan et al., 2009b; Allard et al., 2014), Several studies (Chen et al., 2007; Fan et al., 2009a; Liu et al., 2011; Chen et al., 2013) have suggested to use fully coupled Atmosphere-wave-ocean model for accurate hurricane predictions as well as corresponding ocean responses. However, these studies only validated the wave models using integrated parameters such as the significant wave height and dominant/mean wavelength and direction. The actual two-dimensional wave spectra produced by the wave models are not validated against observations.

The waves are young and highly nonstationary and nonuniform in hurricanes. Under such circumstance, the momentum flux across the air-sea interface depends mainly on short wind waves. Since the momentum flux is a vector sum of the momentum contributions in all frequencies and directions of the wave spectrum, the shape of the wave spectra will directly affect the magnitude of the stress.

The intensity of the hurricane is a balance between enthalpy flux and drag at the sea surface. The hurricane-ocean interaction

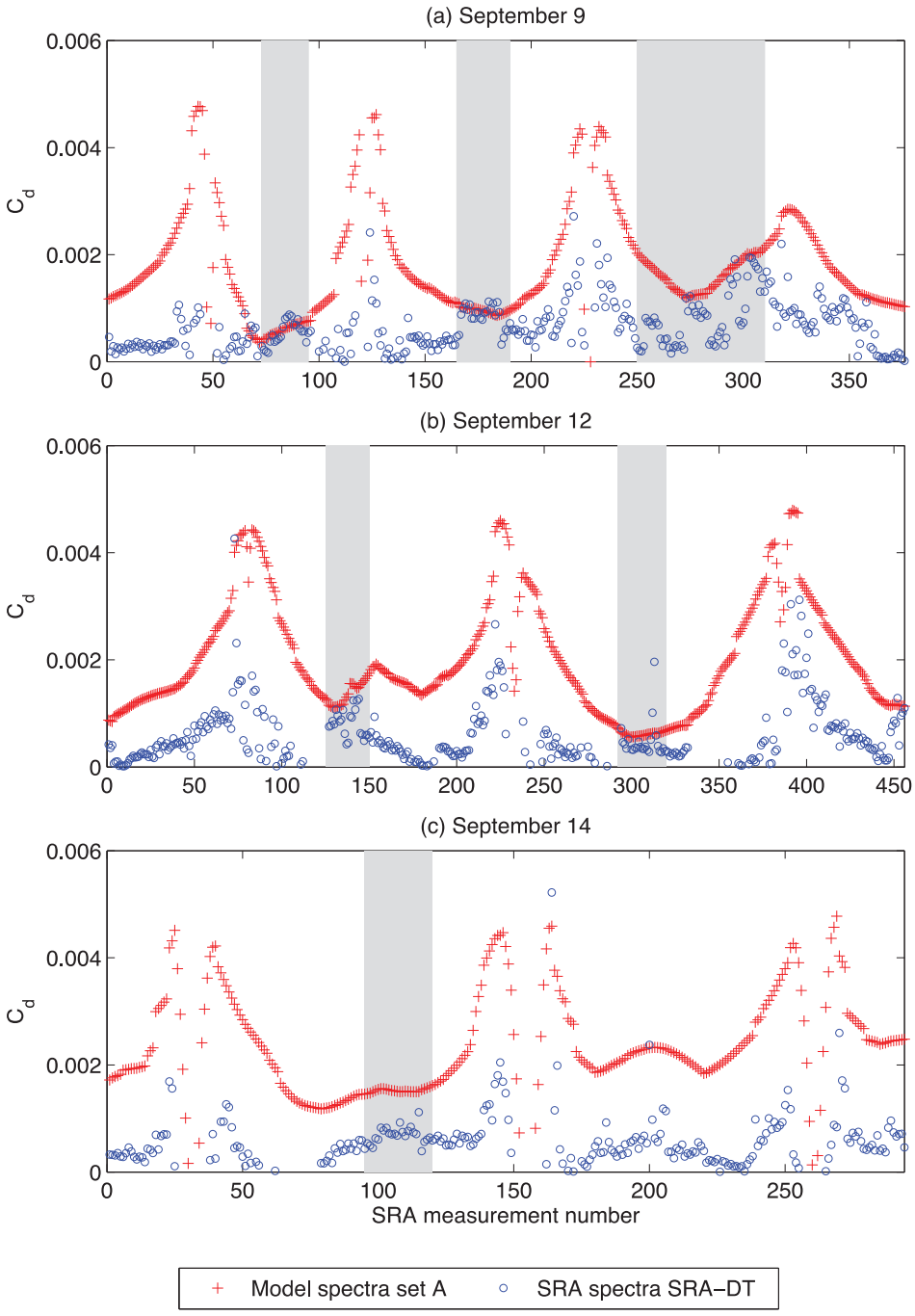

Fig. A1. Drag coefficient (C_d) calculated from model spectra set A (red cross), and constructed SRA spectra SRA-DT along the flight track of (a) September 9, (b) September 12, and (c) September 14. The gray areas are defined the same as in Fig. 4. (For interpretation of the references to color in this figure legend, the reader is referred to the web version of this article.)

can be described as a weather system with positive and negative feedbacks (Ginis, 2002). The primary energy source driving the storm is the evaporation of warm water from the ocean surface and subsequent latent heat release due to condensation during cloud formation. As the storm intensifies, increasing wind speed enhances the evaporation rate, thereby increasing the latent heat energy available for further intensification. However, as the storm continues to intensify, the increasing wind stress on the ocean's surface generates stronger turbulent mixing in the upper oceanic mixed layer. Increased mixing deepens the mixed layer and reduces the SST, hence causing a reduction of sea surface heat and moisture flux. This reduction may in turn decrease the intensity of the storm. Thus, accurate predictions of sea surface and subsurface structures are essential for improving numerical hurricane intensity forecasting (Bender and Ginis, 2000). To do so, we need to have accurate estimate of the drag coefficient. The results in this study indicate that WAVEWATCH III with currently available wind forcing is not ready for this task.

The modeled wind sea part, which is essential for stress calculations, is more problematic than the swells. Several possible reasons could contribute to this discrepancy. First of all, the HRD winds used to force the wave model are created by compiling all available observations relative to the storm center, including land, sea, space, and air-borne platforms. Time and space

interpolation/average are used to create this product, which thus is smoother than real hurricane winds and do not have the fine structures.

Secondly, the Donelan et al. (2006) wind input source functions used in the wave model is supported by measurements taken only under low to moderate wind conditions (Snyder et al., 1981, Donelan et al., 2006). It may not be suitable for high wind conditions such as the hurricanes. Alternate drag calculations were conducted using the Donelan et al. (2012) source function that was developed for hurricane conditions. Although the magnitude of the drag coefficients is reduced, the discrepancy in the rear quadrants of the hurricane remains the same.

Furthermore, the dissipation terms in the model are not developed with any specific attention to the unique conditions of tropical cyclones. They may generate too little dissipation for the swells and too much dissipation for the wind sea under high wind conditions. This would result in modeled wind sea part of the spectra are continuous (unimodal) and narrower in frequency space compared to observations, as we have observed here. More research is required to better understand the source and dissipation terms in the wave model under these complicated extreme weather conditions.

6. Conclusions

In this study, we calculated the drag coefficients using the scanning radar altimeter (SRA) measured two dimensional wave spectra obtained during hurricane Ivan in 2004 and compared them with the drag calculated using WAVEWATCH III produced wave spectra. Donelan et al. (2006) source function is used for the drag calculation. High frequency tail of $f^{-4.5}$ are added to the SRA spectra to extend the frequency range from 0.17 Hz to 1 Hz. This treatment is demonstrated to be able to properly represent the high frequency tails calculated by the wave model.

The drag coefficients disagree between the SRA and model spectra mainly in the right/left rear quadrant of the hurricane where the observed spectra appear to be bimodal while the model spectra are single peaked with more energy in the swell frequencies and less energy in the wind sea frequencies. These results suggest that WAVEWATCH III is currently not capable of providing sensible stress calculations in the rear quadrants of the hurricane.

Acknowledgments

The authors would like to express their appreciation to Dr. Zhitao Yu and the anonymous reviewers for very helpful comments and suggestions. We thank the WAVEWATCH III® development team for developing the code used in this study. NOAA/NWS/EMC/WAVEWATCH III public release version 4.18 is used to generate the data for this study. This work was funded by the Office of Naval Research under program element 0602435 N. This paper is contribution NRL/JA/7320-15-2644 and has been approved for public release.

Appendix A. Drag calculation using Donelan et al. (2012) source function

Donelan et al. (2012) constructed a new wave model for hurricane conditions. The calibration factors (proportionality constants of the source functions) are determined from a comparison of modeled and observed significant wave height and mean period. The source function in their model is given as

$$S_{in} = A_1\left(U_{\lambda/2}cos\theta - c - ucos\phi - vsin\phi\right)U_{\frac{\lambda}{2}}cos\theta - c - ucos\phi - vsin\phi\frac{k\omega}{g}\frac{\rho_a}{\rho_w}E(k,\phi)$$

where, $U_{\lambda/2}$ is the wind speed at a height of one half wavelength, $\lambda/2$; θ is the angle between wind direction and wave direction, ϕ, at wave number k; ω is the frequency; c is the phase speed; E is the wave number-directional variance spectrum; ρ_a is the air density; ρ_w is the water density; and g is the acceleration due to gravity.

This source function is used to calculate drag coefficients using the SRA spectra set SRA-DT and the model spectra set A-DT. The magnitude of these drag coefficients are much lower than that calculated using the Donelan et al. (2006) source function (Fig. A1). However, the variations of both drag coefficient sets are very similar to what we observed in Fig. 4: the A-DT calculated C_d rapidly decreases when the flight heading is away from the center and reaches its minimum along the flight fragments highlighted by gray on Fig. 3, while the SRA-DT calculated C_d increases along these flight fragments (Gray highlighted area in Fig. A1 and Fig. 4).

References

Allard, R., Rogers, E., Martin, P., Jensen, T., Chu, P., Campbell, T., Dykes, J., Smith, T., Choi, J., Gravois, U., 2014. The US navy coupled ocean-wave prediction system. Oceanography 27 (3), 92–103 http://dx.doi.org/10.5670/oceanog.2014.71.

Andreas, E.L., 2004. Spray stress revisited. J. Phys. Oceanogr. 34, 1429–1440.

Banner, M.L., Peirson, W.L., 1998. Tangential stress beneath wind-driven air-water interfaces. J. Fluid Mech. 364, 115–145.

Bender, M.A., Ginis, I., 2000. Real-case simulations of hurricaneocean interaction using a high-resolution coupled model: effects on hurricane intensity. Mon. Wea. Rev. 128, 917–946.

Liu, B., Liu, H., Xie, L., Guan, C., Zhao, D., 2011. A coupled atmosphere–wave–ocean modeling system: simulation of the intensity of an idealized tropical cyclone. Mon. Wea. Rev. 139, 132–152 doi: http://dx.doi.org/10.1175/2010MWR3396.1.

Booij, N., Ris, R.C., Holthuijsen, L.H., 1999. A third-generation wave model for coastal regions, part 1: model description and validation. J. Geophys. Res. 104 (C4), 7649–7666.

Chen, S.S., Zhao, W., Donelan, M.A., Price, J.F., Walsh, E.J., 2007. The CBLAST-hurricane program and the next-generation fully coupled atmosphere–wave–ocean models for hurricane research and prediction. Bull. Amer. Meteor. Soc. 88, 311–317.

Chen, S.S., Zhao, W., Donelan, M.A., Tolman, H.L., 2013. Directional wind-wave coupling in fully coupled atmosphere-wave-ocean models: results from CBLAST-Hurricane. J. Atmos. Science 70, 3198–3215. doi:10.1175/JAS-D-12-0157.1.

Donelan, M.A., Curcic, M., Chen, S.S., Magnusson, A.K., 2012. Modeling waves and wind stress. J. Geophys. Res. 117, C00J23. doi:10.1029/2011JC007787.

Donelan, M.A., Babanin, A.V., Young, I.R., Banner, M.L., 2006. Wave-follower field measurements of the wind-input spectral function. Part II: parameterization of the wind input. J. Physi. Oceanogr. 36, 1672–1688.

Donelan, M.A., Haus, B.K., Reul, N., Plant, W.J., Stiassnie, M., Graber, H.C., Brown, O.B., Saltzman, E.S., 2004. On the limiting aerodynamic roughness of the ocean in very strong winds. Geophys. Res. Lett. 31, L18306. doi:10.1029/2004/GL019460.

Donelan, M.A., Hamilton, J., Hui, W.H., 1985. Directional spectra of wind-generated waves. Phil. Trans. R. Soc. Lond. A315, 509–562.

Emanuel, K., 2003. Tropical cyclones. Annu. Rev. Earth Planet. Sci. 31, 75–104. doi:10.1146/annurev.earth.31.100901.141259.

Fan, Y., Ginis, I., Hara, T., 2009a. The effect of wind-wave-current interaction on air-sea momentum flux and ocean response in tropical cyclones. J. Phys. Oceanogr. 39, 1019–1034. doi:10.1175/2008JPO4066.1.

Fan, Y., Ginis, I., Hara, T., Wright, C.W., Walsh, E.J., 2009b. Numerical simulations and observations of surface wave fields under an extreme tropical cyclone. J. Phys. Oceanogr. 39, 2097–2116. doi:10.1175/2009JPO4224.1.

Ginis, I., 2002. Tropical cyclone-ocean interactions. Atmosphere-Ocean Interactions. In: Perrie, W. (Ed.). In: Advances in Fluid Mechanics Series, 33. WIT Press, pp. 83–114.

Hanson, J.L., Phillips, O.M., 2001. Automated analysis of ocean surface directional wave spectra. J. Atmos. Oceanic Techn. 18, 177–293.

Hasselmann, S., et al., 1988. The WAM model—a third-generation ocean wave prediction model. J. Phys. Oceanogr. 18, 1775–1810. doi:10.1175/1520-0485(1988)018.

Holthuijsen, L.H., Tolman, H.L., 1991. Effects of the Gulf Stream on ocean waves. J. Geophys. Res. 96, 12755–12771.

Janssen, P.A.E.M., 1991. Wave-induced stress and the drag of air flow over sea waves. J. Phys. Oceanogr. 19, 745–754.

Makin, V.K., 2005. A note on the drag of the sea surface at hurricane winds. Boundary-Layer Meteorol. 115, 169–176.

Makin, V.K., Kudryavtsev, V.N., 1999. Coupled sea surface atmosphere model, 1. Wind over waves coupling. J. Geophys. Res. 104 (C4), 7613–7623.

Moon, I.-J., Ginis, I., Hara, T., Tolman, H., Wright, C.W., Walsh, E.J., 2003. Numerical simulation of sea-surface directional wave spectra under hurricane wind forcing. J. Phys. Oceanogr. 33, 1680–1706.

Phadke, A.C., Martino, C.D., Cheung, K.F., Houston, S.H., 2003. Modeling of tropical cyclone winds and waves for emergency management. Ocean Eng. 30, 553–578.

Powell, M.D., Vickery, P.J., Reinhold, T.A., 2003. Reduced drag coefficient for high wind speeds in tropical cyclones. Nature 422, 279–283.
Snyder, R.L., Dobson, F.W., Elliot, J.A., Long, R.B., 1981. A field study of wind generation of ocean waves. J. Fluid Mech. 102, 1–59.
Tolman, H.L., WAVEWATCHIII development group, 2014: User manual and system documentation of WAVEWATCH III version® 4.18 (http://polar.ncep.noaa.gov/waves/wavewatch/manual.v4.18.pdf)
Tolman, H.L., 1998. Validation of a new global wave forecast system at NCEP. In: Edge, B.L., Helmsley, J.M. (Eds.), Ocean Wave Measurements and Analysis. ASCE, pp. 777–786.
Tracy, B., Devaliere, E.-M., Nicolini, T., Tolman, H.L., Hanson, J.L., 2007. Wind sea and swell delineation for numerical wave modeling. In: Proceedings of 10th International Workshop on Wave Hindcasting and Forecasting and Coastal Hazard Symp. Oahu, HI, U.S. Army Engineer Research & Development Center, P12.
Tsagareli, K.N., Babanin, A.V., Walker, D.J., Young, I.R., 2010. Numerical investigation of spectral evolution of wind waves. Part I: wind input source function. J. Phys. Oceanogr. 40, 656–666.
Walsh, E.J., et al., 2002. Hurricane directional wave spectrum spatial variation at landfall. J. Phys. Oceanogr. 32, 1667–1684.
Wright, C.W., et al., 2001. Hurricane directional wave spectrum spatial variation in the open ocean. J. Phys. Oceanogr. 31, 2472–2488.
Xu, F., Perrie, W., Toulany, B., Smith, P.C., 2007. Wind-generated waves in hurricane Juan. Ocean Mod. 16, 188–205. doi:10.1016/j.ocemod.2006.09.001.
Young, I.R., 2006. Directional spectra of hurricane wind waves. J. Geophys. Res. 111. doi:10.1029/2006JC003540.